First real-time isotopic characterisation of N_2O from chemodenitrification

Jing Wei [a,b*], Erkan Ibraim [b], Nicolas Brüggemann [a], Harry Vereecken [a], Joachim Mohn [b]

[a] *Forschungszentrum Jülich GmbH, Institute of Bio- and Geosciences, Agrosphere (IBG-3), Wilhelm-Johnen-Straße, 52425 Jülich, Germany*

[b] *Empa, Swiss Federal Laboratories for Materials Science and Technology, Laboratory for Air Pollution & Environmental Technology, Überlandstrasse 129, 8600 Dübendorf, Switzerland*

***** Corresponding author: *E-mail address, jing.wei@empa.ch (J. Wei); Tel.: +41 58 765 4512; Fax: +41 58 765 1122*

Abstract

Chemodenitrification can be a substantial abiotic source of nitrous oxide (N_2O) in soil. The isotopic signature of N_2O from this process could support source partitioning, but it is currently unknown in sufficient detail. In this study, we determined the isotopic composition of N_2O, produced by the reaction of nitrite (NO_2^-) with lignin, four lignin derivatives, and three types of soils, online with a quantum cascade laser absorption spectrometer (QCLAS). We present the first dataset of continuous measurements of $\delta^{15}N^{bulk}$ ($\delta^{15}N^{bulk} \equiv (\delta^{15}N^{\alpha} + \delta^{15}N^{\beta})/2$), $\delta^{18}O$, and site preference (SP_{N2O}, $SP_{N2O} \equiv \delta^{15}N^{\alpha} - \delta^{15}N^{\beta}$) of N_2O from chemodenitrification in both chemical assays and soils. Considerable amounts of N_2O were produced by chemical reduction of NO_2^-, indicating that chemodenitrification could dominate N_2O emission in NO_2^--rich environments. The values of SP_{N2O} varied by more than 20‰ in the reactions of sodium nitrite with organic substances. Contrary to the common assumption that SP_{N2O} values are constant for a distinct N_2O source process, our results reveal a considerable shift in SP_{N2O} over time for most experiments. The large SP_{N2O} variability might be explained by the multiple pathways with hyponitrous acid or nitramide as N_2O precursors. These findings provide important new information to improve our understanding about the dependency of N_2O isotopic signatures on N_2O production processes.

Keywords: Chemodenitrification; Nitrous oxide; Site preference; Nitrite; Lignin derivatives

TOC Art

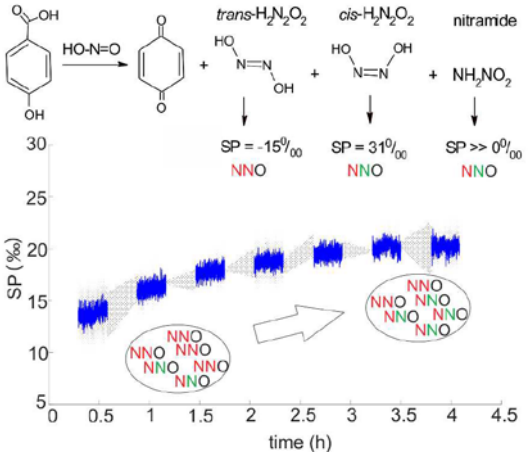

1. INTRODUCTION

Nitrous oxide (N_2O), whose radiative efficiency in the troposphere is almost 300-fold higher than that of carbon dioxide, is the third most important long-lived greenhouse gas contributing about 6% to total anthropogenic global warming (IPCC, 2013). Furthermore, N_2O can decompose to nitric oxide (NO), which further reduces ozone to oxygen, through photolysis in the stratosphere, hence N_2O is also contributing to the depletion of the ozone layer (Ravishankara et al., 2009). After successful emission reduction of chlorine- and bromine-containing halocarbons supported by the Montreal protocol, N_2O currently represents the single most important ozone-depleting substance and it is likely to remain the largest one in the 21st century (Ravishankara et al., 2009). However, the N_2O global mixing ratio has increased by 21% up until 2015 (328 ppb) compared with the pre-industrial level and is still increasing by around 0.89 ppb yr^{-1}, mainly due to the use of nitrogen fertiliser in agriculture (WMO, 2016). Therefore, it is currently imperative to mitigate global N_2O emissions, which would require a better understanding of relevant N_2O production pathways.

For a long period of time, microbial nitrification and denitrification conducted by bacteria, fungi and archaea have been considered as the main N_2O source processes. During nitrification, ammonium (NH_4^+) is first oxidised to hydroxylamine (NH_2OH) by ammonium oxidisers, which is afterwards oxidised to nitrite (NO_2^-) under the catalyst of hydroxylamine oxidoreductase (HAO), while N_2O is released as a byproduct of either biotic or abiotic NH_2OH oxidation (Caranto and Lancaster, 2017; Liu et al., 2017; Stein, 2011). In the case of denitrification including bacterial, fungal, and nitrifier denitrification, N_2O is considered as an obligatory intermediate or end product of biotic reduction of NO_2^- (Stein, 2011; Sutka et al., 2008). However, NO_2^- can be released through both nitrification and denitrification into the soil and rapidly chemically reduced to N_2O by soil organic matter (SOM) or transition metals, which is termed as chemodenitrification (Chalk and Smith, 1983). Acidic conditions largely promote chemodenitrification processes because the chemical reactivity of nitrous acid (HNO_2), formed through the protonation of NO_2^-, is much higher than that of the NO_2^- ion itself (Chalk and Smith, 1983). Increasing evidence demonstrates that N_2O emission from chemodenitrification can be substantial in

various ecosystems, including extreme arid and cold lakes, ponds, and soils (Ostrom et al., 2016; Peters et al., 2014; Samarkin et al., 2010), temperate forests and arable lands (Venterea, 2007; Wei et al., 2017a), and sediments (Wankel et al., 2017). Therefore, the contribution of chemodenitrification to global N_2O emissions could have been largely underestimated.

Stable isotope techniques offer a powerful tool to disentangle N_2O production pathways in the environment. Since the two nitrogen atoms are located asymmetrically in the linear N_2O molecule ($N^{\beta}N^{\alpha}O$), the difference of $\delta^{15}N$ between the α and β position is defined as site preference ($SP_{N2O} \equiv \delta^{15}N^{\alpha} - \delta^{15}N^{\beta}$) (Toyoda and Yoshida, 1999). Independent of the isotopic composition of the substrates, SP_{N2O} has been thought to be very specific for a certain N_2O production pathway and represents the transient state of the N_2O formation and reduction (Toyoda and Yoshida, 1999; Toyoda et al., 2002). Microbial N_2O sources of nitrification and fungal denitrification, as well as chemical oxidisation of NH_2OH, feature relatively high SP_{N2O} values of 27 - 40‰ (Heil et al., 2014; Heil et al., 2015; Rohe et al., 2014; Sutka et al., 2003; Sutka et al., 2006; Sutka et al., 2008; Toyoda et al., 2005), while bacterial denitrification and nitrifier denitrification are characterised by low SP_{N2O} values of -11 to 1.4‰ (Frame and Casciotti, 2010; Sutka et al., 2003; Sutka et al., 2006; Toyoda et al., 2005). The reduction of N_2O to N_2 by heterotrophic denitrifiers is characterised by an isotopic enrichment factor for SP_{N2O} of -5.0 to -6.8‰ (Lewicka-Szczebak et al., 2017; Ostrom et al., 2007).

The $\delta^{15}N^{bulk}$ values of N_2O are highly influenced by the isotope effects of both N_2O production and reduction. During nitrification, the ^{15}N in N_2O is enriched by -0.3–5.7‰ for NH_2OH oxidation (Sutka et al., 2003; Sutka et al., 2006), but depleted by 18.6–68‰ and 12.3–34.3‰ for NH_4^+ oxidation by ammonia oxidizing bacteria (AOB) and ammonia oxidizing archaea (AOA), respectively (Frame and Casciotti, 2010; Jung et al., 2014; Mandernack et al., 2009; Yamazaki et al., 2014). In contrast, N_2O is ^{15}N-depleted by 10–37‰ and 30.9–45.6‰ during nitrate (NO_3^-) reduction by denitrifying bacteria and fungi, respectively (Rohe et al., 2014; Sutka et al., 2006; Toyoda et al., 2005). When NO_2^- is reduced to N_2O, N_2O is ^{15}N-depleted by 31.4–39.5‰ for nitrifier denitrification and by 8.5–29.0‰ for fungal denitrification (Rohe et al., 2014; Sutka et al., 2003; Sutka et al., 2008; Yoshida, 1988). In addition, the

reduction of N_2O to N_2 by heterotrophic denitrifiers is accompanied by a 4.1–6.6‰ decrease in $\delta^{15}N$ due to the isotope effect of N-O bond cleavage (Lewicka-Szczebak et al., 2017; Ostrom et al., 2007).

Despite the depletion of ^{15}N, ^{18}O is generally enriched in N_2O by 3–12.6‰ for nitrification (Jung et al., 2014; Santoro et al., 2011), and by 4–23‰ and 13.2–33.3‰ for NO_3^- reduction to N_2O by denitrifying bacteria and fungi, respectively (Rohe et al., 2014; Toyoda et al., 2005). ^{18}O enrichment of N_2O ranges from 34.2 to 60.8‰ for NO_2^- reduction during fungal denitrification and was found to be 8.4‰ during nitrifier denitrification (Frame and Casciotti, 2010; Rohe et al., 2014). The O exchange of reaction intermediates with water is a key factor affecting the fractionation effect of ^{18}O (Kool et al., 2007; Kool et al., 2009; Kool et al., 2011). Significant differences in ^{18}O exchange were observed between bacterial and fungal denitrification (Lewicka-Szczebak et al., 2016), varying from 17 to 94% depending on the N_2O production pathways and environmental conditions (Rohe et al., 2017). Based on the above-mentioned results, N_2O isotopic signatures have been widely used to partition N_2O sources for wastewater treatment systems (Harris et al., 2015; Wunderlin et al., 2013) and natural ecosystems from local (Bol et al., 2003; Toyoda et al., 2009; Toyoda et al., 2011; Wolf et al., 2015) to global scales (Röckmann and Levin, 2005; Snider et al., 2015; Toyoda et al., 2013).

In spite of the fact that chemodenitrification accounts for substantial N_2O emissions in certain ecosystems, its N_2O isotopic signature has not been investigated in sufficient detail (Ostrom et al., 2016; Zhu-Barker et al., 2015). Moreover, the currently reported N_2O isotopic signatures of chemodenitrification are discordant with each other for varying reaction conditions. The reported SP_{N2O} values include: 10 to 22‰ for the abiotic reduction of NO_2^- by ferrous iron (Fe^{2+}) at neutral pH when oxygen is limiting (Jones et al., 2015), 20 to 26‰ for the chemical reaction of NO_2^- with SOM at pH 3.8 (Wei et al., 2017a), around 30‰ for the reaction of NO_2^- with trimethylamine-borane at pH 1 (Toyoda et al., 2005), and 34 to 35‰ for the chemical reaction of NH_2OH with NO_2^- at pH 3–6 (Heil et al., 2014). Thus, more sophisticated studies are needed to explain this large variability, as well as to evaluate its use for N_2O source attribution.

Lignin is a phenolic polymer accounting for 20% of organic carbon in the terrestrial biosphere, and its degradation in soil produces various phenolic compounds which are chemically highly reactive to NO_2^- (Thevenot et al., 2010). It has been reported that the NO_2^- related N_2O emission is positively correlated to the lignin content in acidic organic-rich forest soils (Wei et al., 2017a). Therefore, the reaction of lignin and its derivatives with NO_2^- might play a key role in chemodenitrification. A previous study showed that the SP_{N2O} of abiotic reactions of NO_2^- with lignin derivatives varied largely depending on pH and lignin-derived reactants (Wei et al., 2017b). The question of whether SP_{N2O} remain constant during NO_2^- reduction by SOM is vital for a process-level understanding and interpretation of potential reaction mechanisms. To answer this question, we investigated the N_2O isotopic signatures from reactions of NO_2^- with five lignin-derived compounds in real time, as well as NO_2^--related N_2O emissions in three types of soils for the first time by laser spectroscopy. In addition to N_2O, other by-products of the reaction, i.e. NO and phenols, were investigated with chemiluminescence and gas chromatography-mass spectrometry, respectively, to further elucidate the reaction mechanisms.

2. MATERIALS AND METHODS

2.1. Laser spectroscopic analysis of N_2O isotopic composition

The analyser used in this study was a commercially available quantum cascade laser absorption spectrometer (QCLAS, CW-QC-TILDAS-76-CS; Aerodyne Research Inc., Billerica, USA) that has been customised for simultaneous analysis of the four most abundant N_2O isotopic species, i.e. $^{14}N^{14}N^{16}O$, $^{14}N^{15}N^{16}O$, $^{15}N^{14}N^{16}O$, and $^{14}N^{14}N^{18}O$ (Ibraim et al., 2018). The QCLAS comprises a continuous-wave mid-infrared quantum cascade laser source (Alpes Lasers SA, Switzerland) emitting at 2203 cm^{-1} and an astigmatic multi-pass absorption cell with a path length of 76 m and a cell volume of 0.62 L. Laser control, data acquisition, and quantification of the N_2O isotopic species are performed using TDL Wintel (Aerodyne Research Inc., Billerica, USA). The QCLAS was operated in a flow-through mode with a temporal resolution of 1 Hz for data acquisition. The Allan variance precision of the spectrometer for

ratios of isotopic species R^{α}, R^{β}, and R^{18O} with 1250 s spectral averaging was less than 0.1‰ (1 σ standard deviation) (Werle et al., 1993). The gas flow through the QCLAS gas cell was adjusted to 12 mL min^{-1} and the cell pressure was kept at 26.67 ± 0.01 hPa using a pressure controller (MKS Instruments, Andover, MA, USA).

The isotope ratios of samples were corrected using a two-point calibration approach with calibration gas 1 (Cal1, $\delta^{15}N^{\alpha}$ = -22.21 ± 0.39‰ vs. air-N_2, $\delta^{15}N^{\beta}$ = -49.28 ± 0.40‰ vs. air-N_2, $\delta^{18}O$ = 26.94 ± 0.23‰ vs. VSMOW) and calibration gas 2 (Cal2, $\delta^{15}N^{\alpha}$ = -0.13 ± 0.28‰ vs. air-N_2, $\delta^{15}N^{\beta}$ = 1.35 ± 0.29‰ vs. air-N_2, $\delta^{18}O$ = 38.46 ± 0.15‰ vs. VSMOW) at 36 ppm. Both Cal1 and Cal2 were prepared in synthetic air (20.5% of O_2, 79.5% of N_2, 99.999% purity, Messer Schweiz AG, Switzerland) as described in Waechter et al. (2008) and calibrated against standard gases which were primarily analysed by Sakae Toyoda at Tokyo Institute of Technology (Mohn et al., 2014; Toyoda and Yoshida, 1999). To account for drift effects of the QCLAS, Cal1, diluted to 35 ppm N_2O, was analysed at least every 35 min for 10 min. Nonlinearity effects of N_2O concentration on isotope ratios were determined, before and after each experiment, analysing Cal1 at 12, 25, 36, 45, 54, 68, 82 ppm N_2O and corrected as described below. The selection of sample versus calibration gas was conducted by two 3-way solenoid valves (series 9, Parker Hannifin, USA).

2.2. Experimental setup

The experimental setup for online measurement of N_2O isotopocules is illustrated in Fig. 1. A quartz glass chamber with a PTFE cover plate was used as the reaction chamber. To decrease the delay time and increase the real-time response of the system, the volume of the reaction chamber was reduced to 300 mL by inserting a hollow polypropylene cylinder. In addition, a fan was installed at the top of the chamber to ensure that the headspace gas phase was homogenously mixed. The absence of significant leaks (pressure drop < 100 Pa min^{-1} at 0.1 MPa overpressure) was assured with a leak test before every experiment. Gas flows in the setup were controlled using mass flow controllers (MFCs, Redy Smart series, Vögtlin Instruments, Switzerland) and a number of two- and three-position solenoid

159 valves (Parker Hannifin Corp., USA). The experimental setup was controlled via a custom-written
160 LabVIEW code (National Instruments Corp., USA), and devices were connected via a 16-port serial-to-
161 ethernet network connector (Etherlite 160, Digi International Inc., USA).

162 The reactor was continuously purged with 14–16 mL min^{-1} of synthetic air (20.5% of O_2, 79.5% of
163 N_2, 99.999% purity, Messer Schweiz AG, Switzerland) to deliver the liberated process gases into the
164 spectrometer gas cell. The sample gas was dehumidified using a Nafion permeation dryer (MD-050-
165 72S-1, Perma Pure, USA) and the overflow which was not subjected to laser spectroscopic analysis was
166 exhausted into a fume hood, thereby keeping the pressure of the reaction chamber constant at
167 ambient pressure. Carbon monoxide (CO) was removed with a Sofnocat oxidation catalyst (Sofnocat
168 423, Molecular Products Ltd., United Kingdom), as CO would otherwise induce spectral interferences
169 during QCLAS analysis. Thereafter, carbon dioxide (CO_2) was removed from the process gas with a trap
170 containing 13.8 g of ascarite (10–35 mesh, Fluka, Switzerland) bracketed with magnesium perchlorate
171 ($Mg(ClO_4)_2$, 2 × 3.5 g, Fluka, Switzerland) and separated with glass wool (BGB Analytics AG, Switzerland).
172 If N_2O concentrations in the sample gas were above 82 ppm, the gas was diluted by adding an
173 additional flow of synthetic air through MFC1 and the N_2O concentration in the undiluted process gas
174 was back-calculated by multiplying the measured N_2O concentration with the dilution factor. Since co-
175 production of nitric oxide (NO) was expected together with N_2O, the absence of spectral interferences
176 by NO was assured by a pre-test, where 50 ppm NO was added to a N_2O calibration gas and no
177 significant change in the analysed N_2O isotopic composition was observed.

178

179 **2.3. Experimental procedure**

180 Sodium nitrite ($NaNO_2$, VWR, Germany) was used as the NO_2^- source, and its $\delta^{15}N$ (-18.00 ± 0.08‰
181 vs. air-N_2) and $\delta^{18}O$ (10.09 ± 0.05‰ vs. VSMOW) were measured using an elemental analyser coupled
182 to an isotope ratio mass spectrometer (EA-IRMS, Flash EA 2000 and Delta V Plus; Thermo Fisher
183 Scientific, Bremen, Germany). Common lignin-derived compounds, organosolv lignin (Chemical Point
184 UG, Oberhaching, Germany), 4-hydroxybenzoic acid, 4-hydroxy-3-methoxybenzoic acid, 4-hydroxy-

3,5-dimethoxybenzoic acid, and 4-hydroxy-3,5-dimethoxybenzaldehyde (VWR, Germany) (Wei et al., 2017b), were chosen as model substances in this study. All chemicals were reagent grade or better. Forest and grassland soils were sampled from the O_a layer of the Wüstebach catchment (50°30'15"N, 6°18'15"E) and the Rollesbroich grassland (50°37'0"N, 6°26'0"E), respectively, in the northern Eifel region, Germany. The sites are part of the German environmental monitoring programme, named TERENO (Zacharias et al., 2011). Agricultural soil was sampled from the top layer (0–20 cm) of the Hohenschulen experimental farm (54°19'05"N, 9°58'38"E) at the University of Kiel, Germany. The characteristics of all soils are listed in Table 1.

A 100-mL beaker containing 5–26 g of carbon substances or soil together with a stir bar was placed into the chamber. Then, the whole setup was flushed using 18 mL min^{-1} of synthetic air until the N_2O concentration declined and stabilised at < 0.1 ppm. Afterwards, 50 mL of $NaNO_2$ solution in ultrapure water (18.2 MΩ cm) was injected into the beaker through a rubber septum on top of the chamber. A magnetic stirrer was used to mix the reactants for 5 min. Experimental details for each treatment including the amount of carbon substances/soils and $NaNO_2$ and flow rate of the carrier gas are listed in Table 2. Different substrate-to-nitrite ratios were chosen to reach the calibrated N_2O concentration range (12−82 ppm), and higher N_2O mixing ratios (>80 ppm) were diluted by manually adding a dilution flow of synthetic air. For sterilisation treatments, soils were distributed in portions of 10 g each into 50 mL glass bottles with screw caps (VWR, Germany) and autoclaved for 30 min at 1.2 bar and 121°C, and $NaNO_2$ solution and carrier gas were passed through a 0.2 µm PTFE filter. The online measurements of N_2O isotopic signatures lasted for 4-6 h, and all experiments were conducted in triplicate. pH was measured at an interval of 25-90 min using a pH meter (model 720, Orion Research, Inc., Jacksonville, Florida, USA).

2.4. Analysis of N_2O and NO_x emissions and organic reaction products

In a separate set of experiments, N_2O and nitrogen oxide (NO_x) emissions were analysed by a combination of a dual quantum cascade laser absorption spectrometer (QCLAS, DUAL CW RT-QC-

TILDAS-76, Aerodyne Research, Inc., Billerica, MA, USA) and a chemiluminescence based analyser (CLD, AC32M, Ansyco GmbH, Karlsruhe, Germany). In each experiment, 0.5 g of lignin or 0.3 mmol of lignin derivatives was placed into a 100 mL beaker in a reaction chamber of 2 L volume. The system was purged with 3 L min^{-1} of synthetic air (20.5% oxygen and 79.5% nitrogen) until N_2O and NO_x signals decreased to below 0.1 and 0.01 ppb, respectively. Then, 100 mL of 1 mM sodium nitrite (VWR, Germany) solution was injected into the reaction beaker and the mixing ratios of NO_x and N_2O were recorded with temporal resolution of 5 s and 1 s, respectively.

The organic products of the reactions of NO_2^- with 4-hydroxy-3-methoxybenzoic acid, 4-hydroxy-3,5-dimethoxybenzoic acid, and lignin were determined using a gas chromatography-mass spectrometry (GC-MS). In detail, 0.06 mmol of lignin derivative (4-hydroxy-3-methoxybenzoic acid or 4-hydroxy-3,5-dimethoxybenzoic acid) or 0.1 g of lignin was placed into a 22.5 mL gas chromatography vial containing 5 mL of 0.1 mM $NaNO_2$ solution and the mixture was incubated for 24 h at room temperature. Afterwards, the products were extracted with 2 mL of methanol through solid phase extraction using a C18-bonded monolithic silica column (Bond Elut C18, 500 mg, 3 mL; VWR, Germany) and afterwards measured with a GC-MS (5973N, Agilent, Santa Clara, California ,USA) (Kaiser and Benner, 2012).

2.5. Data analysis

N_2O isotope ratios (R^{α}, R^{β} and R^{18O}) were calculated based on the concentrations of $^{14}N^{14}N^{16}O$, $^{14}N^{15}N^{16}O$, $^{15}N^{14}N^{16}O$, and $^{14}N^{14}N^{18}O$ obtained from QCLAS (section 2.1):

$$R^{\alpha} = \frac{^{14}N^{15}N^{16}O}{^{14}N^{14}N^{16}O} \quad (1)$$

$$R^{\beta} = \frac{^{15}N^{14}N^{16}O}{^{14}N^{14}N^{16}O} \quad (2)$$

$$R^{18O} = \frac{^{14}N^{14}N^{18}O}{^{14}N^{14}N^{16}O} \quad (3)$$

A drift correction was applied to all isotope ratios based on regular measurements of Cal1 at 36 ppm N_2O. Thereafter, isotope ratios were converted to the δ-notation in per mille by applying the following formula:

$$\delta_{A/B} = \left(\frac{R_A}{R_B} - 1\right) \times 1000‰ \quad (4)$$

2-point calculation was applied using Cal1 as the working standard according to Gröning (2018):

$$r\delta_{sam/std} = \delta_{sam/cal1} \times \frac{\delta_{cal2/std} - \delta_{cal1/std}}{\delta_{cal2/cal1}} + \delta_{cal1/std} \quad (5)$$

In Eq. (5), sam, std, cal1, and cal2 denote sample gas, international standard (air-N_2 for $^{15}N/^{14}N$, and VSMOW for $^{18}O/^{16}O$), and calibration gas 1 and 2, respectively, $r\delta_{sam/std}$ is the raw δ value of sample without a correction of N_2O concentration dependency. Third-order polynomial regressions were applied to correct for the dependency of $\delta^{15}N^{\alpha}$, $\delta^{15}N^{\beta}$, and $\delta^{18}O$ on N_2O concentration (Figure S1). Two regression equations were defined: f_{low} for the N_2O range of 12–45 ppm, and f_{high} for the N_2O range of 36–83 ppm. The R^2 values were higher than 0.99 for both f_{low} and f_{high}, and the differences of δ values calculated by f_{low} and f_{high} at intermediate N_2O concentrations from 36 to 45 ppm were lower than 0.5‰ (Figure S2), which indicates that both f_{low} and f_{high} were well fitted. The N_2O concentration dependency was corrected according to the following equation:

$$\delta_{sam/std} = r\delta_{sam/std} + f(C_{cal1}) - f(C_{sam}) \quad (6)$$

In Eq. (6), $r\delta_{sam/std}$ is the raw δ value of the sample calculated based on Eq. (5), C_{cal1} is the average concentration of all the Cal1 measurements at around 36 ppm, C_{sam} denotes the N_2O mixing ratio of the sample, and f denotes f_{low} when C_{sam} is equal to or lower than 36 ppm, but f_{high} when C_{sam} is higher than 36 ppm. Finally, $\delta^{15}N^{bulk}$ was calculated as the average of $\delta^{15}N^{\alpha}$ and $\delta^{15}N^{\beta}$:

$$\delta^{15}N^{bulk} \equiv (\delta^{15}N^{\alpha} + \delta^{15}N^{\beta}) / 2 \quad (7)$$

while SP_{N2O} was determined using:

$$SP_{N2O} \equiv \delta^{15}N^{\alpha} - \delta^{15}N^{\beta} \quad (8)$$

Net isotope effects $\Delta^{15}N(N_2O/NO_2^-)$ and $\Delta^{18}O(N_2O/NO_2^-)$ were calculated as the difference of δ values of N_2O from that of NO_2^-, and then normalised based on the N_2O concentration:

$$\Delta^{15}N(N_2O/NO_2^-) = \sum((\delta^{15}N_{N2O}^{bulk} - \delta^{15}N_{NO_2^-}) \times C_{N_2O}) / \sum C_{N_2O} \quad (9)$$

$$\Delta^{18}O(N_2O/NO_2^-) = \sum((\delta^{18}O_{N2O} - \delta^{18}O_{NO_2^-}) \times C_{N_2O})/\sum C_{N_2O} \quad (10)$$

The relative N_2O emission rate X_{N2O} (μmol N_2O mol^{-1} NO_2^- mol^{-1} s^{-1} for lignin compounds and μmol N_2O mol^{-1} NO_2^- kg^{-1} s^{-1} for soil samples), was normalised for the reactants as follows:

$$X_{N2O} = \frac{C_{N2O} \times P \times F}{M_{NO_2^-} \times R \times T \times m} \quad (11)$$

C_{N2O} is the mixing ratio of N_2O (ppm) measured in real time at 1 Hz, *P* denotes the pressure in the reaction chamber (101325 Pa), *F* represents the flow rate of the carrier gas (ml s^1), *R* is the ideal gas constant (8.314 m^3 Pa mol^{-1} K^{-1}), *T* represents the temperature of the headspace in the reaction chamber (293.15 K), M_{NO2-} is the total applied NO_2^- (mol), and m is the amount of lignin compounds or soil (mol for lignin compounds and kg for soil). The manual dilution of N_2O mixing ratio with synthetic air was corrected with either a dilution factor or polynomial curve fitting. All of the calculations were conducted using MATLAB R2014b (MathWorks, Inc., USA).

3. RESULTS

3.1. N_2O isotopic composition from reactions of NO_2^- with lignin derivatives

In the reaction of NO_2^- with organosolv lignin, approximately 8% of NO_2^- was converted to N_2O within 4 h, accounting for the highest relative N_2O emission rate (Fig. 2a). Compared with organosolv lignin, the reactions of NO_2^- with lignin-derived acids and aldehyde were much slower, with relative N_2O emission rates of less than 900 μmol N_2O mol^{-1} NO_2^- mol^{-1} s^{-1}. The average relative N_2O emission rate decreased in the order: 4-hydroxy-3,5-dimethoxybenzoic acid > 4-hydroxybenzoic acid > 4-hydroxy-3-methoxybenzoic acid > 4-hydroxy-3,5-dimethoxybenzaldehyde (Table 3). In addition, the temporal trend of N_2O emission differed between lignin derivatives: the relative N_2O emission rate peaked within 1.2 h and decreased quickly afterwards in the treatment of 4-hydroxy-3,5-dimethoxybenzoic acid (Fig. 2m), while it took about 3 h to reach the maximum in the experiment with 4-hydroxybenzoic acid (Fig. 2e). By contrast, the reaction rate changed gradually in the experiments with 4-hydroxy-3-methoxybenzoic acid and 4-hydroxy-3,5-dimethoxybenzaldehyde (Figs. 2i and 2q). pH increased by one unit in the first 4 h of the experiments with 4-hydroxybenzoic acid, 4-hydroxy-3-

methoxybenzoic acid, and 4-hydroxy-3,5-dimethoxybenzoic acid, while it remained between approximately 2.7 and 6.1 in the experiments with organosolv lignin and 4-hydroxy-3,5-dimethoxybenzaldehyde, respectively.

A large variability of SP_{N2O} values (from 4.6 ± 1.7‰ to 28.9 ± 8.8‰) was observed in reactions of NO_2^- with lignin and lignin-derived acids as well as aldehyde (Table 1). Most interestingly, SP_{N2O} values of the same reaction also changed substantially over time. In the first 4 h, SP_{N2O} values increased by approximately 5‰ in the treatment of 4-hydroxy-3,5-dimethoxybenzaldehyde (Fig. 2r), while they increased by more than 10‰ in the treatment of organosolv lignin (Fig. 2b). By contrast, no clear temporal trend was observed for the reaction of NO_2^- with 4-hydroxy-3-methoxybenzoic acid with SP_{N2O} values ranging from 10 to 15‰ during the whole experiment (Fig. 2j). The SP_{N2O} fluctuated largely by approximate 10‰ over time in the reaction of NO_2^- with 4-hydroxybenzoic acid and 4-hydroxy-3,5-dimethoxybenzoic acid (Figs. 2f and 2n).

The temporal trends of $\delta^{18}O$ and $\delta^{15}N^{bulk}$ of N_2O also differed in the reactions of NO_2^- with lignin and the four lignin-related compounds: both $\delta^{18}O$ and $\delta^{15}N^{bulk}$ of N_2O remained relatively stable in the experiments with 4-hydroxy-3-dimethoxybenzoic acid and 4-hydroxy-3,5-dimethoxybenzaldehyde, however, they varied by more than 12‰ in the reactions of NO_2^- with organosolv lignin and 4-hydroxybenzoic acid (Fig. 2). Correspondingly, the concentration-weighted net isotope effects $\Delta^{15}N(N_2O/NO_2^-)$ and $\Delta^{18}O(N_2O/NO_2^-)$ varied from -20.1 to -10.0‰ and from 10.2 to 19.5‰, respectively, in the reactions of NO_2^- with lignin derivatives (Table 3). No significant Rayleigh effects could be observed due to the low conversion ratio of NO_2^- to N_2O.

3.2. NOx emission and organic products from the reactions of NO_2^- with lignin derivatives

Considerable NO_x emission was observed in the reactions of NO_2^- with lignin derivatives, and NO_x emission increased to the maximum within 20 min, which was 1–2 h before N_2O reached its maximum (Fig. 3). In the reaction of NO_2^- with lignin, GC-MS analysis revealed the existence of various phenolic products including phenol, 3-methylphenol, 2-methoxyphenol, 4-ethylphenol, 2-methoxy-4-

methylphenol, 4-ethyl-2-methoxyphenol, 2-methoxy-4-vinylphenol, 2,6-dimethoxyphenol, 2,6-dimethoxy-4-methylphenol, 2-methoxy-4-(1-propenyl)phenol, and 2,6-demethoxy-4-[(1E)-prop-1-en-1-yl]phenol (Fig. 4a). While 2-methoxyphenol, 4-hydroxy-2-methoxybenzaldehyde, and 4-hydroxy-3-methoxybenzoic acid methyl ester were formed in the reaction of NO_2^- with 4-hydroxy-3-methoxybenzoic acid (Fig. 4b), and 2,6-dimethoxyphenol and 4-hydroxy-3,5-dimethoxybenzohydrazide were formed in the reaction of NO_2^- with 4-hydroxy-3,5-dimethoxybenzoic acid (Fig. 4c).

3.3. N_2O isotopic signatures from NO_2^- reactions in soils

N_2O emissions from soil samples varied from approximately 0.73 to 5.64 μmol N_2O mol^{-1} NO_2^- kg^{-1} soil s^{-1} in the order: forest soil > grassland soil > agriculture soil, and sterilisation did not inhibit the N_2O emissions (Table 3). The concentration-weighted SP_{N2O} values ranged from 17.9 ± 3.2‰ to 25.7 ± 2.3‰ in soils, which was within the SP_{N2O} range of NO_2^- reactions with lignin derivatives (Table 3). Similar to the treatments of lignin and its derivatives, temporal changes in SP_{N2O} by more than 6‰ were observed in forest, grassland, and agricultural soils (Fig. 5). In contrast, the variability of $\delta^{18}O$ and $\delta^{15}N^{bulk}$ between soil types was much smaller compared with SP_{N2O} (Fig. 5). The real-time $\Delta^{15}N(N_2O/NO_2^-)$ varied from -30 to -20‰ and from -27.7 to -21.9‰ in non-sterilised and sterilised soils, while $\Delta^{18}O(N_2O/NO_2^-)$ changed from 14.4 to 22.5‰ and from 14.8 to 21.4‰ in non-sterilised and sterilised soils, respectively (Table 3).

4. DISCUSSIONS

4.1 N_2O production pathways

Two different pathways, a hyponitrous acid pathway or a nitramide pathway (Fig. 6), have been discussed in relation to NO and N_2O formation from the reaction of NO_2^- with lignin derivatives (Austin, 1961; Kainz and Huber, 1959), which might therefore explain the different N_2O production rates and shifting SP_{N2O} values. Taking 4-hydroxybenzoic acid as an example, NO_2^- is first protonated to HNO_2,

338 and the carboxyl group (-COOH) is subsequently substituted by a nitroso group (-NO) from HNO_2 to
339 form CO_2 and 4-nitrosophenol (compound 1). The elimination of –COOH should account for the
340 increase of pH in the treatments of 4-hydroxybenzoic acid, 4-hydroxy-3-methoxybenzoic acid, and 4-
341 hydroxy-3,5-dimethoxybenzoic acid (Fig. 2). As 4-nitrosophenol is unstable at acidic pH, it partly
342 decomposes to phenol (compound 4) and NO, while the other part is transformed to *p*-benzoquinone
343 4-oxime (compound 2) through rearrangement (Austin, 1961; Stevenson and Swaby, 1964). The
344 formation of NO was confirmed in our experiments by high NO emission at the onset of the reactions
345 measured with a chemiluminescence based analyser (Fig. 3). Similarly, 2-methoxyphenol and 2,6-
346 dimethoxyphenol were detected as a product in the treatment of 4-hydroxy-3-methoxybenzoic acid
347 (Fig. 4b) and 4-hydroxy-3,5-dimethoxybenzoic acid (Fig. 4c), respectively, which further confirmed the
348 decarboxylation and the following removal of the nitroso group. Subsequently, the phenol can be
349 attacked by another HNO_2 molecule through electrophilic substitution, resulting in the formation of 2-
350 nitrosophenol (compound 5), which can rearrange to compound 6.
351 In the hyponitrous acid pathway, the C=N double bond of oximes can be subject to electrophilic
352 attack of HNO_2 with a nitroso group being attached to the nitrogen atom and a hydroxyl group binding
353 to the carbon atom, leading to the formation of hydroxyl-nitroso compounds (compounds 3 and 7)
354 (Austin, 1961). Hydroxyl-nitroso compounds are very unstable and decompose quickly to hyponitrous
355 acid (compound 8 and 9) and benzoquinones, with hyponitrous acid decomposing to N_2O (Austin,
356 1961). In the nitramide pathway, electrophilic substitution, instead of electrophilic addition, occurs at
357 the nitrogen atom of the oximes with the production of nitramines (compounds 10 and 11), which
358 decompose quickly to benzoquinones and nitramide (compound 12), and nitramide further
359 decomposes to N_2O (Kainz and Huber, 1959). With the consumption of NO_2^- and 4-hydroxybenzoic acid,
360 as well as the decomposition of nitroso compounds, pH slowly increased and the formation rate of N_2O
361 decreased (Fig. 2).
362 The number and position of electrophilic functional groups attached to the aromatic ring can affect
363 the reaction kinetics through mesomeric (+/-M) and inductive (+/-I) effects, as well as steric effects.

On the one hand, a methoxy group (-OCH_3) enhances the electron density of the aromatic ring by its +M effect, facilitating the electrophilic attack by HNO_2 (or more precisely by the resulting nitrosonium ion NO^+) especially in the ortho and para positions relative to the methoxy group, thereby accelerating the reaction. On the other hand, -OCH_3 also hinders the formation of oximes to some extent through a steric effect, thus inhibiting N_2O production. In addition, acidic pH favours the protonation of NO_2^-, thereby promoting the reaction rate of NO_2^- with lignin compounds. Therefore, we hypothesise that the mesomeric and inductive effects can explain the much higher N_2O emission rate in the 4-hydroxy-3,5-dimethoxybenzoic acid treatment than in the 4-hydroxybenzoic acid treatment in the first hour of the reaction, while the higher pH could explain the lower N_2O production rate 2 h later (Figs. 2e and 2m). Even though the methoxy group in 4-hydroxy-3-methoxybenzoic acid increases the aromatic electron density, the increase in electron density is less pronounced as in 4-hydroxy-3,5-dimethoxybenzoic acid. This, in combination with the inhibitory steric effect of the methoxy group and the higher pH, could be the reason why the N_2O emission rate did not increase in the 4-hydroxy-3-methoxybenzoic acid treatment compared with 4-hydroxybenzoic acid in the first 3 h (Figs. 2e and 2i). In the case of 4-hydroxy-3,5-dimethoxybenzaldehyde, the aldehyde group first has to be oxidized to a carboxyl group before decarboxylation can occur on the one hand, and the pH higher than 6.0 limits the protonation of NO_2^- on the other hand. Therefore, the N_2O emission rate was much lower in the experiment with 4-hydroxy-3,5-dimethoxybenzaldehyde compared with 4-hydroxy-3,5-dimethoxybenzoic acid (Figs. 2m and 2q). Since organosolv lignin is extracted with an organic solvent as one of the alternative chemical wood pulping techniques (Wei et al., 2017b), it has a higher content of reactive functional groups compared with other lignin derivatives (Fig. 4). The various reactive functional groups as well as the very low pH in the experiment with organosolv lignin helps to explain the drastically higher N_2O emission rate (Fig. 2a).

4.2. N_2O isotopic signatures depending on reaction conditions

4.2.1 SP_{N2O}

Real-time measurements of SP_{N2O} from the reactions between NO_2^- and lignin derivatives over 4–6 hrs resulted in concentration-weighted average SP_{N2O} values between 13.4 ± 3.8‰ and 24.4 ± 1.0‰ (Table 3). This is comparable to an earlier off-line study, where a large variability of SP_{N2O} values (11.9–30‰) has been observed (Wei et al., 2017b). Remaining differences in SP_{N2O} might be explained by a substantial longer incubation period in previous off-line experiments (24 h) (Wei et al., 2017b) in comparison to measurements conducted in the present study (4–6 h). SP_{N2O} values for the reaction of NO_2^- with lignin derivatives observed in both studies (Wei et al., 2017b) also coincide with the ones collected from reactions of NO_2^- with SOM fractions at pH 3 (20–26‰) (Wei et al., 2017a), the chemical reduction of NO_2^- by ferrous iron at pH 7 under anaerobic conditions (10–22‰) (Jones et al., 2015), and the reaction of NO_2^- with trimethylamine borane at pH 1 (~30‰) (Toyoda et al., 2005). The significant progress in the present study, to the best of our knowledge, provides the first real-time dataset of SP_{N2O} values for a number of exemplary reactions, which revealed a shift in SP_{N2O} during the reactions. In the following, these temporal trends are discussed with respect to N_2O production pathways. Isotope effects of N_2O reduction are not considered, since it is very unlikely that N_2O is further reduced to N_2 during chemodenitrification under oxic conditions.

According to the N_2O reaction mechanisms proposed above (Fig. 6), hyponitrous acid and nitramide are supposed to be the direct precursors of N_2O formation from the reaction of NO_2^- with lignin derivatives. For the symmetric hyponitrous acid molecule, isotope effects during its decomposition are probably the key factor controlling SP_{N2O} values. Theoretical calculations using density functional theory (DFT) calculations by Fehling and Friedrichs (2011) predict the formation of both *cis*- and *trans*-hyponitrous acid, and substantially different SP_{N2O} values for N_2O formation via both intermediates. While a low SP_{N2O} value is predicted for the reaction via *trans*-hyponitrous acid (-15‰), a much higher value is assumed for *cis*-hyponitrous acid decomposition (31‰) (Fehling, 2012). In principle, the formation of *trans*-hyponitrous acid from hydroxyl-nitroso compounds is favoured due to steric effects, however, *trans*-hyponitrous acid could be isomerised to *cis*-hyponitrous acid through a fast acid-base equilibrium which generally dominates under strongly acidic conditions (Bringas et al., 2016; Fehling

and Friedrichs, 2011). Hyponitrous acid is also proposed as the key precursor in microbial N_2O production. During the oxidation of NH_2OH to N_2O by HAO, a NH_2OH molecule is first bound to the enzyme, then a second NH_2OH molecule attacks the N atom of the first, leading to the formation of a *cis*-hyponitrous acid-like N-N bond (Yamazaki et al., 2014). Finally, N_2O with a SP_{N2O} value of 30–36‰ is generated through the cleavage of the OH group of the first NH_2OH molecule (Yamazaki et al., 2014). The NO reduction by fungal NO reductase (NOR) to N_2O follows a mechanism that is similar with the NH_2OH oxidation by HAO, as two NO molecules are sequentially bound to NOR and form a *cis*-hyponitrite-like compound which decomposes quickly to N_2O with a SP_{N2O} of 35–37‰ (Obayashi et al., 1998; Rohe et al., 2014; Sutka et al., 2008). By contrast, during bacterial denitrification, two NO molecules are simultaneously bound to the enzyme and a *trans*-hyponitrite-like compound is formed (Watmough et al., 2009), which further decomposes to N_2O with a SP_{N2O} of around zero.

In the nitramide pathway, the N atoms of the first- and second-bound nitroso group act as the terminal (N^{β}) and central (N^{α}) nitrogen atoms of the N_2O molecule, respectively. Nitramide formation is the rate-determining step, hence kinetic isotope effects during nitramide formation are supposed to dominate the N_2O isotopic composition. Since the cleavage of the N=C bond favours $^{15}N^{\beta}$ depletion but the formation of the N-N bond of nitramines favours $^{15}N^{\alpha}$ enrichment, we speculate that the SP_{N2O} value via the nitramide pathway should be significantly higher than zero. Consequently, both the nitramide and *cis*-hyponitrous acid pathways favour higher SP_{N2O}, while the *trans*-hyponitrous acid pathway favors lower SP_{N2O}. The temporal changes of SP_{N2O} values could result from the varying ratio of N_2O being produced via the *trans*-hyponitrous acid with respect to the sum of N_2O produced via nitramide and *cis*-hyponitrous acid.

The electrophilic attack and the formation of hyponitrous acid can be facilitated by acidic pH. By contrast, the formation of nitramide is favoured at higher pH. Therefore, the increase in pH could account for the dramatic drop of N_2O production rate, accompanied by an increase of SP_{N2O}, at the end of the experiment with 4-hydroxybenzoic acid and 4-hydroxy-3,5-dimethoxybenzoic acid (Fig. 2).

4.2.2 Net isotope effects

The net ^{15}N isotope effect, $\Delta^{15}N$ (N_2O/ NO_2^-), observed in this study is within the range of values reported in previous studies on chemodenitrification (Grabb et al., 2017; Jones et al., 2015; Wei et al., 2017b), but slightly higher than that of nitrifier denitrification (Sutka et al., 2006). Isotope effects are affected by the reaction kinetics and they are generally determined by the rate-limiting step (Snider et al., 2009), such as the formation of hyponitrous acid and nitramide in the reactions of lignin derivatives with NO_2^-. The cleavage of ^{14}N-C to form hyponitrous acid and ^{14}N=C to form nitramide are preferred over the cleavage of ^{15}N-C and ^{15}N=C bonds. Therefore ^{15}N depletion was observed in the chemical reduction of NO_2^- to N_2O by lignin derivatives (Table 3). Even though N_2O reduction leads to an increase of $\delta^{15}N^{bulk}$ of the remaining N_2O pool by 2-7‰ (Ostrom et al., 2007), this process is not relevant during chemodenitrification, hence the variation of $\Delta^{15}N$ (N_2O/ NO_2^-) during the reactions of this study (Fig. 2) are likely resulting from the dynamic change of hyponitrous acid and nitramide formation rates, dependent on substrate availability and pH.

The concentration-weighted net ^{18}O isotope effect, $\Delta^{18}O$ (N_2O/ NO_2^-), ranged from 10.2 to 20.2‰ (Table 3), which is in a similar range of previously reported values (Grabb et al., 2017; Jones et al., 2015; Wei et al., 2017b). The value of $\Delta^{18}O$ (N_2O/ NO_2^-) found in the present study is much higher than that of nitrifier denitrification (Sutka et al., 2006), but much lower than that of fungal denitrification (Rohe et al., 2014; Sutka et al., 2008). Apart from the kinetic isotope effect of N_2O production, $\Delta^{18}O$ (N_2O/ NO_2^-) is also strongly influenced by O exchange with water. Depending on different N_2O production mechanisms, O exchange of substrates with water can vary from approximately 2% to more than 90% (Kool et al., 2007). In the reactions of lignin derivatives with NO_2^-, O exchange could occur both between nitrite itself and water and between the hydroxyl groups of hyponitrous acid and nitramide. However, the rate and degree of O exchange during formation of hyponitrous acid and nitramide are currently unclear and should be explored in future studies.

4.3 Chemodenitrification and N_2O source partitioning

4.3.1 Chemodenitrification in soil

Recently, increasing evidence is provided for the central role of NO_2^- in the soil N cycle and particularly in N_2O emission (Maharjan and Venterea, 2013; Venterea, 2007). In the present study, we also found that NO_2^- led to N_2O emission in all of the three types of soils (Fig. 3), equivalent to 43.2–483.8 μmol N_2O mol^{-1} NO_2^- kg^{-1} soil d^{-1}, which is in a similar range as in previous studies where chemodenitrification dominated (Ostrom et al., 2016; Venterea, 2007; Wei et al., 2017a). As NO_2^- -related N_2O production in unsterilised soils may include microbial pathways, e.g. denitrification and nitrifier denitrification, and chemodenitrification (Wankel et al., 2017), sterilised soil samples were also analysed in the present study. Instead of decreasing N_2O production, autoclaving increased the N_2O emission rate dramatically, which could be explained by an increased solubility of SOM after autoclaving, accelerating the reactivity of the soil to NO_2^- (Berns et al., 2008). In addition, the values of SP_{N2O}, $\delta^{18}O$, and $\delta^{15}N^{bulk}$ were within the range of NO_2^--lignin reactions in chemical assays and they changed in a similar trend in sterilised and unsterilised soil samples (Fig. 3), indicating that chemodenitrification was the main N_2O source in soils after NO_2^- application and accounted for the shifts of N_2O isotopic composition.

4.3.2 N_2O source partitioning

Even though SP_{N2O} is widely used for N_2O source partitioning, it still remains an open question of whether it is sufficiently conclusive or not (Decock and Six, 2013; Wei et al., 2017b). The reliability of using isotopic signatures in N_2O source partitioning highly depends on the robustness of N_2O isotopic signatures of certain N_2O production and reduction processes. The ranges of SP_{N2O}, $\delta^{15}N^{bulk}$, and $\delta^{18}O$ have been observed to be 6.0 to 37.4‰, -41.0 to -3.9‰, and 14 to 44.6‰ for chemodenitrification (Jones et al., 2015; Toyoda et al., 2005; Wei et al., 2017b), -11 to 1.4‰, -34.8 to -8.8‰, and 10 to 20‰ for bacterial denitrification (Toyoda et al., 2005; Zou et al., 2014), 34 to 40‰, -34 to -21.9‰, and 30 to 40‰ for fungal denitrification (Sutka et al., 2008), and 27 to 37‰, -61.4 to -40.3‰, and 40 to 50‰

for nitrification (Sutka et al., 2006), respectively (Fig. 7a). Net isotope effects of $\Delta^{15}N(N_2O/NO_2^-)$ and $\Delta^{18}O(N_2O/NO_2^-)$, have been observed in ranges of -28.1 to 9.6‰ and 3 to 24.2‰ for chemodenitrification (Grabb et al., 2017; Jones et al., 2015; Wei et al., 2017b), -39.5 to -31.4‰ and 7.0 to 9.8‰ for nitrifier denitrification (Sutka et al., 2006), and -29.0 to -8.8‰ and 55.8 to 60.8‰ for fungal denitrification (Rohe et al., 2014; Sutka et al., 2008), respectively (Fig. 7b).

Due to the distinct ^{15}N and ^{18}O isotopic effects, $\Delta^{15}N(N_2O/NO_2^-)$ and $\Delta^{18}O(N_2O/NO_2^-)$ of chemodenitrification are clearly separated from the corresponding values of fungal denitrification and nitrifier denitrification (Fig. 7b). Even though $\delta^{15}N^{bulk}$ and $\delta^{18}O$ of N_2O of chemodenitrification are also clearly distinct from bacterial denitrification, they strongly overlap with fungal denitrification and nitrification in the end-member map (Fig. 7a). To date, only few data of $\Delta^{15}N(N_2O/NO_2^-)$ and $\Delta^{18}O(N_2O/NO_2^-)$ from NO_2^--related N_2O production have been published (Rohe et al., 2014; Sutka et al., 2006; Sutka et al., 2008), and further studies are needed to explore the isotope effects of N_2O production under various conditions.

Since the range of SP_{N2O} values of chemodenitrification is in the intermediate zone between fungal denitrification and nitrifier denitrification, a classical two-end-member mixing model (Zhang et al., 2016) fails to quantify N_2O sources unambiguously. Therefore, a more sophisticated model involving both SP_{N2O} and isotope effects is needed for more reliable N_2O source partitioning. Similarly, SP_{N2O} values encompassed the ranges of microbial nitrification (33 to 37‰) and denitrification (-10 to 0‰) in the McMurdo Dry Valleys, Antarctica, even though chemodenitrification accounted for most of the N_2O emission (Peters et al., 2014). Further, the application of SP_{N2O} also failed to attribute source processes of N_2O in Lake Vida, Victoria Valley, Antarctica (Ostrom et al., 2016; Zhu-Barker et al., 2015) and in the Don Juan Pond, Antarctica (Samarkin et al., 2010), where chemodenitrification with distinguishable N_2O isotope signatures acted as the main N_2O source.

5. CONCLUSION

Biotic ammonium oxidisation and nitrate reduction provide NO_2^- sources for chemodenitrification. On the other hand, chemodenitrification and biotic N_2O production processes, including nitrification and denitrification, compete for NO_2^-. In agreement with a previous study (Wei et al., 2017b), we found that SP_{N2O} values of chemodenitrification varied largely in experiments with different lignin derivatives, and end-member maps of N_2O isotopic signatures become highly limited for N_2O source partitioning when chemodenitrification is taken into account. Furthermore, this laboratory study demonstrated that the N_2O isotopic signatures of chemodenitrification also changed over time during the reaction, which contributes to the temporary variation of N_2O isotopic composition in soils. Two different N_2O production mechanisms with hyponitrous acid or nitramide as intermediate would very likely explain the temporal changes of SP_{N2O} during the reactions studied, which deserve to be further explored. Due to the large variability and uncertainty of N_2O isotopic signatures from chemodenitrification, additional constraints, such as a combination of N_2O isotopic composition with N and O isotope effects, novel clumped-isotopes or triple oxygen isotopic information, are needed for making N_2O source partitioning unambiguous.

Table 1. Characteristics of the soil samples. The indicated precision is the standard deviation for replicate sample measurements (n = 3).

Soil sample	Soil pH	Total N (mg g^{-1})	Total C (%)	C/N	WHC [a] (%)	Fe (mg g^{-1})	Mn (mg g^{-1})
Forest soil	3.5 ± 0.0	14.6 ± 0.0	30.1 ± 0.8	20.6 ± 0.6	137.0 ± 0.1	29.0 ± 3.0	2.20 ± 0.12
Grassland soil	5.1 ± 0.0	12.8 ± 0.1	4.62 ± 0.02	3.6 ± 0.1	80.0 ± 1.2	33.5 ± 1.5	1.40 ± 0.40
Agricultural soil	6.0 ± 0.2	1.4 ± 0.1	1.28 ± 0.01	9.1 ± 0.2	35.0 ± 4.2	11.7 ± 0.2	0.46 ± 0.03

Note:
[a] WHC, water holding capacity.

Table 2. Experimental details for individual treatment.

Lignin derivative/soil sample	Lignin derivative (mmol)/soil (g)	Nitrite (mmol)	Water (mL)	Flow rate (mL min^{-1})
organosolv lignin[a]	3.3	0.1 – 0.2	50	16 – 32
4-hydroxybenzoic acid	57.9	20.0	50	16
4-hydroxy-3-methoxybenzoic acid	59.5	23.5	50	16 – 32
4-hydroxy-3,5-dimethoxybenzoic acid	40.4	27.9	50	16 – 32
4-hydroxy-3,5-dimethoxybenzaldehyde	34.0	58.8	50	16
non-sterilised forest soil	10.0	18.8 – 31.8	50	16 – 32
non-sterilised grassland soil	10.0	17.6 – 29.4	50	16
non-sterilised agricultural soil	10.0	17.6 – 29.4	50	16
sterilised forest soil	10.0	29.4 – 35.3	50	12.8 – 16
sterilised grassland soil	10.0	6.5 – 9.2	50	16 – 20
sterilised agricultural soil	10.0	11.8 – 13.5	50	16 – 18.4

Note:
[a] organosolv lignin is estimated as $C_{81}H_{92}O_{28}$ with molecular weight of 1513.6 g mol^{-1} according to PubChem.

Table 3 Net isotope effect of ^{15}N and ^{18}O, N_2O site preference (SP_{N2O}), and N_2O production rate of the reaction of nitrite with different organic compounds and soil samples. Results are shown as the average values ± standard deviation of three replicates.

	$\Delta^{15}N(N_2O/NO_2^-)$ (‰ vs. air-N_2)			$\Delta^{18}O(N_2O/NO_2^-)$ (‰ vs. VSMOW)			SP_{N2O} (‰)			Relative N_2O production rate [c]		
	Max. [a]	Min. [a]	Avg. [b]	Max.	Min.	Avg.	Max.	Min.	Avg.	Max.	Min.	Avg.
Organosolv lignin	-3.1 ± 4.8	-17.8 ± 4.0	-10.0 ± 4.1	21.4 ± 1.2	16.0 ± 0.9	19.5 ± 1.7	28.8 ± 0.2	12.1 ± 1.7	24.4 ± 1.0	940 ± 37	475 ± 156	810 ± 33
4-hydroxybenzoic acid	-7.1 ± 4.5	-22.8 ± 0.8	-15.4 ± 1.2	17.0 ± 2.2	4.7 ± 3.7	10.2 ± 3.4	25.6 ± 1.4	7.7 ± 2.8	19.5 ± 0.5	0.28 ± 0.0	0.10 ± 0.02	0.19 ± 0.02
4-hydroxy-3-methoxybenzoic acid	-14.8 ± 3.9	-20.9 ± 4.2	-17.7 ± 3.9	19.4 ± 4.7	10.3 ± 0.9	13.3 ± 1.6	20.5 ± 6.4	7.3 ± 5.4	13.4 ± 3.8	0.20 ± 0.02	0.08 ± 0.02	0.15 ± 0.01
4-hydroxy-3,5-dimethoxybenzoic acid	-9.9 ± 0.3	-18.3 ± 0.4	-13.0 ± 0.5	20.2 ± 2.9	7.2 ± 2.1	12.2 ± 0.4	28.9 ± 8.8	4.6 ± 1.7	15.4 ± 1.7	0.90 ± 0.11	0.00 ± 0.13	0.33 ± 0.02
4-hydroxy-3,5-dimethoxybenzaldehyde	-17.7 ± 3.8	-22.6 ± 1.9	-20.1 ± 2.8	20.6 ± 3.2	16.5 ± 2.7	18.9 ± 2.8	23.2 ± 3.4	13.7 ± 4.0	19.2 ± 2.6	0.12 ± 0.02	0.09 ± 0.02	0.11 ± 0.02
non-sterilised agricultural soil	-20.0 ± 5.2	-26.6 ± 2.4	-22.7 ± 4.8	22.5 ± 2.7	17.3 ± 3.3	20.2 ± 2.4	31.1 ± 3.3	14.8 ± 0.9	22.1 ± 0.6	0.84 ± 0.12	0.42 ± 0.12	0.55 ± 0.02
sterilised agricultural soil	-24.0 ± 2.8	-27.7 ± 2.2	-25.8 ± 2.6	21.2 ± 2.3	17.6 ± 0.7	19.4 ± 1.3	29.2 ± 4.1	21.3 ± 0.8	25.7 ± 2.3	1.81 ± 1.21	1.03 ± 0.13	1.22 ± 0.27
non-sterilised forest soil	-20.8 ± 5.8	-24.0 ± 5.5	-22.8 ± 5.8	20.6 ± 0.9	16.4 ± 1.3	17.8 ± 1.6	21.2 ± 1.3	15.9 ± 0.8	18.6 ± 1.1	2.51 ± 0.07	1.21 ± 0.48	2.23 ± 0.08
sterilised forest soil	-22.3 ± 0.8	-26.6 ± 0.7	-23.9 ± 0.8	20.3 ± 0.9	14.8 ± 2.4	16.8 ± 1.7	25.9 ± 1.5	17.4 ± 1.4	20.1 ± 0.9	6.06 ± 0.35	3.70 ± 0.38	5.64 ± 0.38
non-sterilised grassland soil	-21.6 ± 4.3	-30.0 ± 2.8	-25.2 ± 3.1	20.9 ± 4.0	14.4 ± 3.4	17.9 ± 3.3	24.8 ± 2.2	12.2 ± 5.1	17.9 ± 3.2	0.92 ± 0.13	0.56 ± 0.20	0.73 ± 0.20
sterilised grassland soil	-21.9 ± 1.6	-25.9 ± 2.6	-23.9 ± 2.1	21.4 ± 1.3	17.4 ± 1.1	19.5 ± 1.2	29.1 ± 1.0	19.2 ± 3.9	23.2 ± 2.7	2.75 ± 0.60	1.99 ± 0.16	2.18 ± 0.18

Note:

[a] Max. and Min. values are the real-time maximum and minimum values, respectively.

[b] Avg. values were concentration-weighted over the complete experimental run.

[c] The unit of relative N_2O production rate is µmol N_2O mol^{-1} NO_2^- mol^{-1} compound s^{-1} for lignin and lignin derivatives, and µmol N_2O mol^{-1} NO_2^- kg^{-1} soil s^{-1} for soil samples

547

548 **Figures**

549

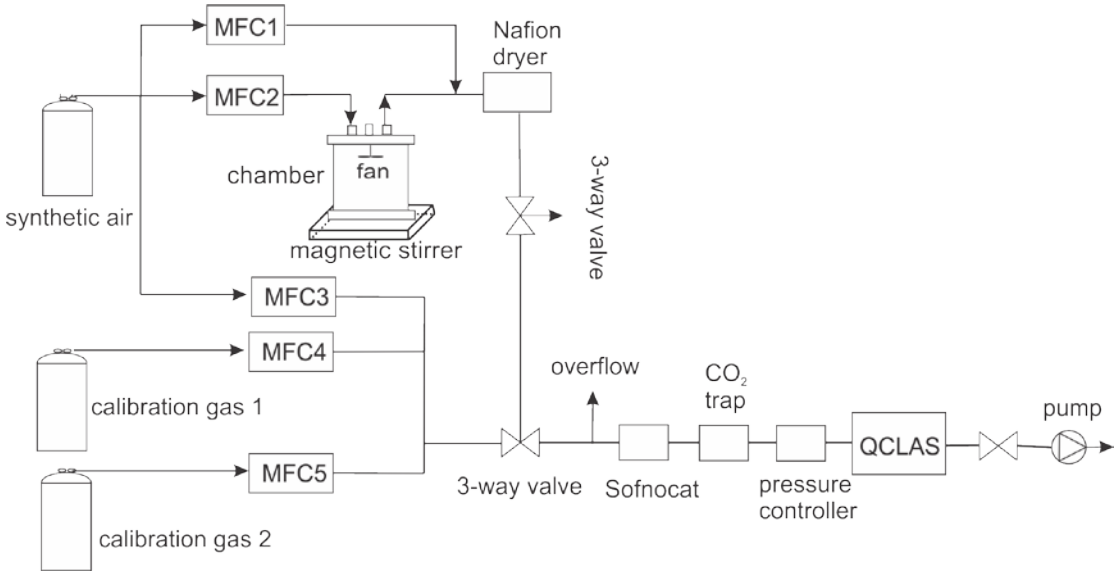

550

551 **Fig. 1.** Schematic diagram of the setup used for real-time measurement of N_2O isotopic signatures.

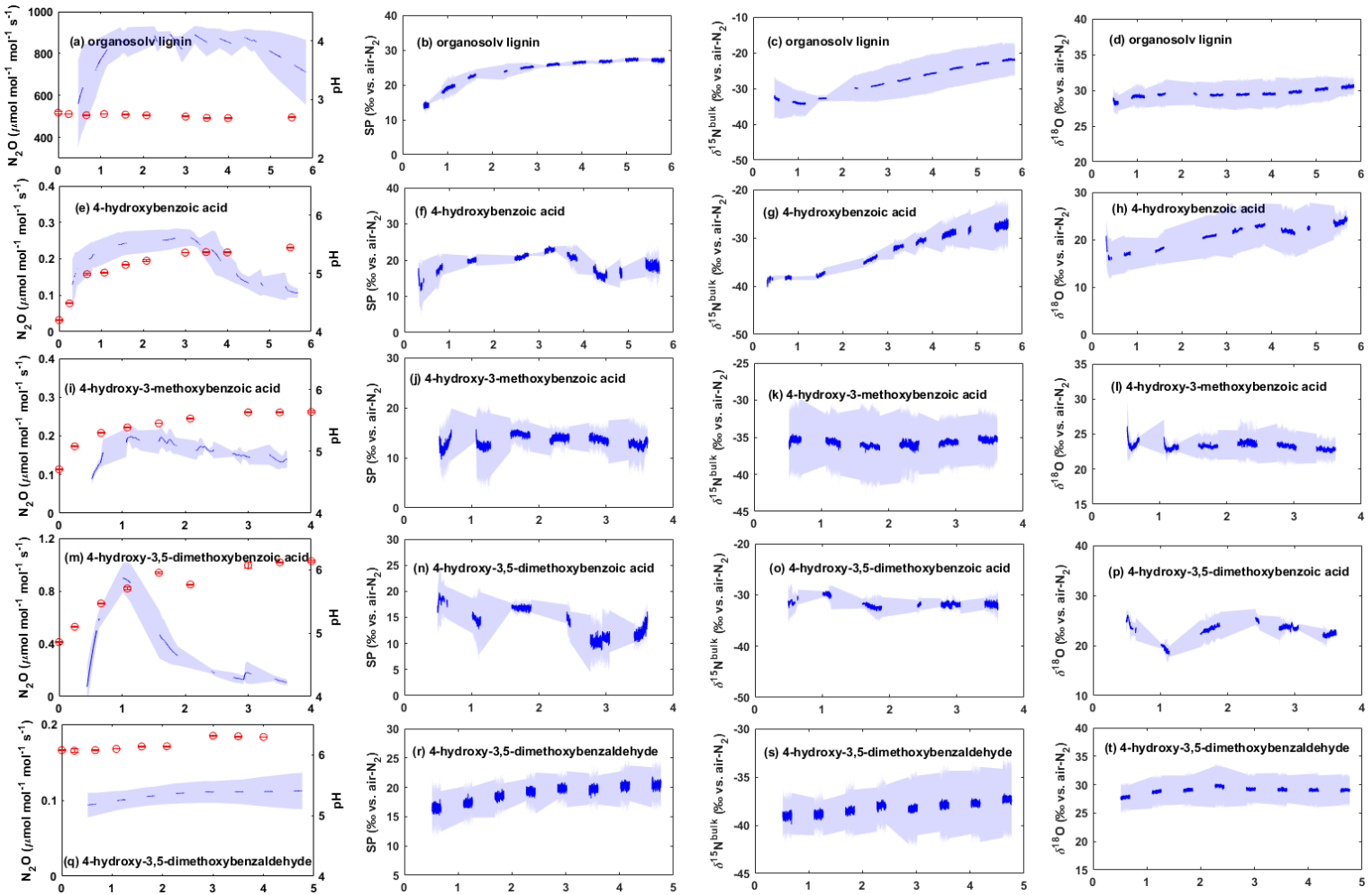

552

553 **Fig. 2**. Reaction of NO_2^- with organosolv lignin and lignin derivatives. Blue dots are the mean N_2O production rates and isotopic signatures of triplicates, the
554 shaded areas indicate the standard deviation (SD), periods without sample measurement are linearly interpolated. Red dots represent mean pH $\pm$ SD of
555 triplicates.

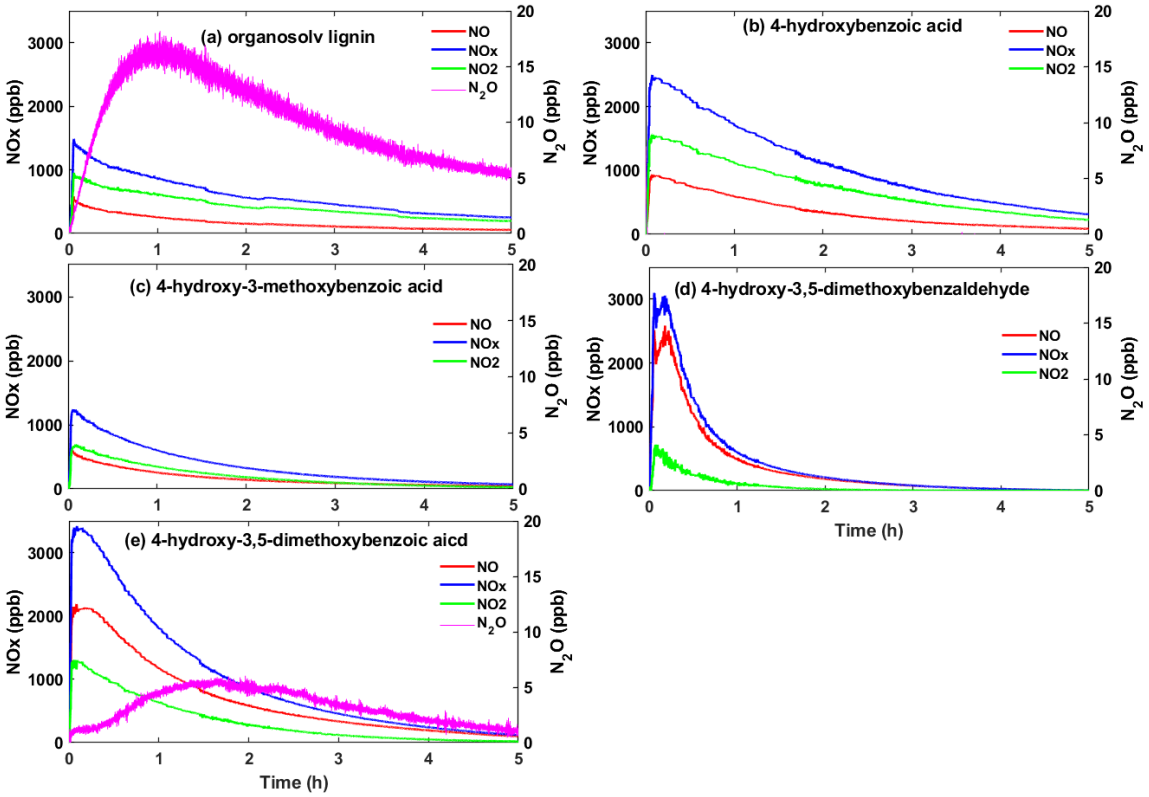

Fig. 3. Simultaneous N_2O and NO_x (NO + NO_2) emissions from the reactions of nitrite with organosolv lignin (a), 4-hydroxybenzoic acid (b), 4-hydroxy-3-methoxybenzoic acid (c), 4-hydroxy-3,5-dimethoxybenzaldehyde (d), 4-hydroxy-3,5-dimethoxybenzoic acid (e). The N_2O mixing ratio in the treatments of 4-hydroxybenzoic acid, 4-hydroxy-3-methoxybenzoic acid, and 4-hydroxy-3,5-dimethoxybenzaldehyde was lower than the detection limit.

565

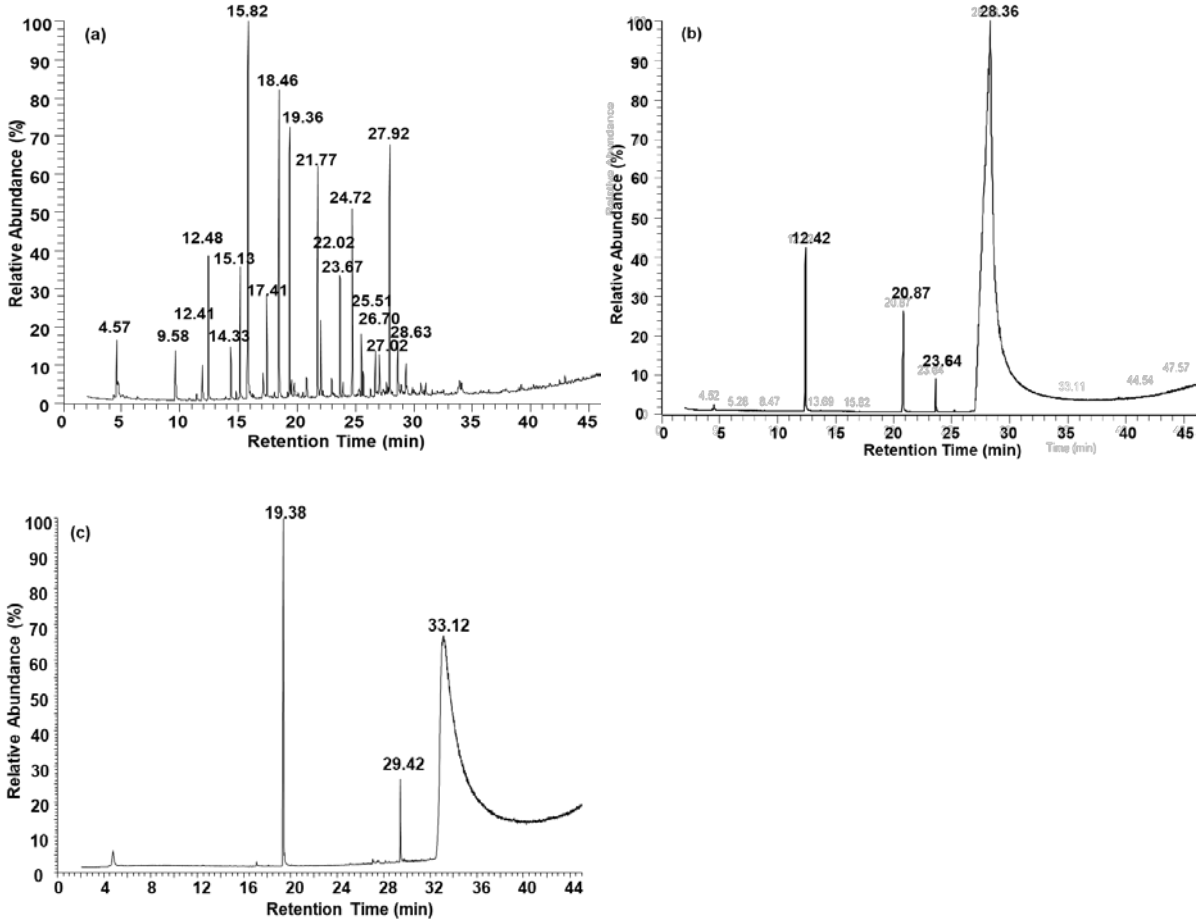

566

567 **Fig. 4**. Gas chromatography–mass spectrometry spectrum of products from the reaction of nitrite with
568 organosolv lignin (a), 4-hydroxy-3-methoxybenzoic acid (b), and 4-hydroxy-3,5-dimethoxybenzoic acid
569 (c). Compounds in (a) represent (2-aziridinylethyl)aminephenol, 3-methylphenol, 2-methoxyphenol, 4-
570 ethylphenol, 2-methoxy-4-methylphenol, 4-methylbenzaldehyde, 4-ethyl-2-methoxyphenol, 2-
571 methoxyl-4-vinylphenol, 2,6-dimethoxyphenol, 2,6-dimethoxy-4-methylphenol, 2-methoxy-4-(1-
572 propenyl)phenol, 1,2,3-trimethoxy-5-methylbenzene, 2-(3,4-dimethoxyphenyl)-6-methyl-3,4-
573 chromanediol, 2,6-demethoxy-4-(1E)-1-propen-1-yl-phenol, 2,6-dimethoxyl-4-(1E)-1-propen-1-yl-
574 phenol, 4-hydroxy-3,5-dimethoxybenzaldehyde, 2,6-dimethoxy-4-(1E)-1-propen-1-yl-phenol, 1-(4-
575 hydroxyl-3,5-dimethoxyphenyl)ethanone at retention time (t_R) of 4.57, 9.58, 12.41, 12.48, 14.33, 15.13,
576 15.82, 17.41, 18.46, 19.36, 21.77, 22.02, 23.67, 24.72, 25.51, 26.70, 27.02, 27.92, 28.63 min,
577 respectively. Compounds in (b) stand for 2-methoxyphenol, 4-hydroxy-2-methoxybenaldehyde, 4-
578 hydroxy-3-methoxybenzoic acid methyl ester, 4-hydroxy-3-methoxybenzoic acid at t_R of 12.42, 20.87,
579 23.64, 28.36 min, respectively. Compounds in (c) are 2,6-dimethoxyphenol at t_R of 19.38 min, 4-
580 hydroxy-3,5-dimethoxybenzohydrazide at t_R of 29.42 min, and 4-hydroxy-3,5-dimethoxybenzoic acid
581 at t_R of 33.12 min.

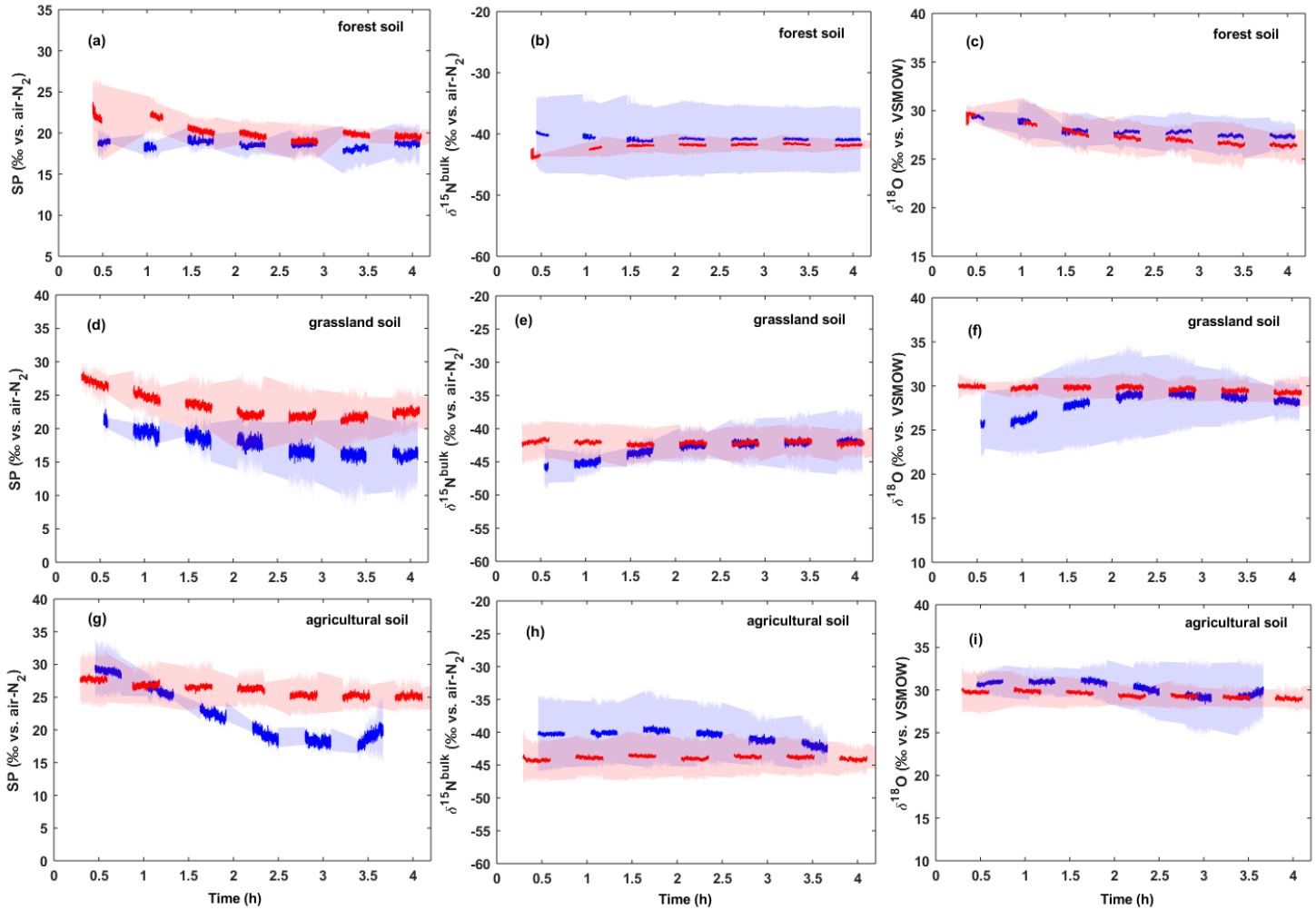

582

583 **Fig. 5**. Isotopic signatures of NO_2^- related N_2O emission in forest, agricultural, and grassland soils. Shown are mean values of three replicates in unsterilized
584 (blue dots) and sterilized (red dots) soils. The shaded areas indicate the standard deviation (SD) of triplicated measurements, periods without measurement are
585 linearly interpolated.

586

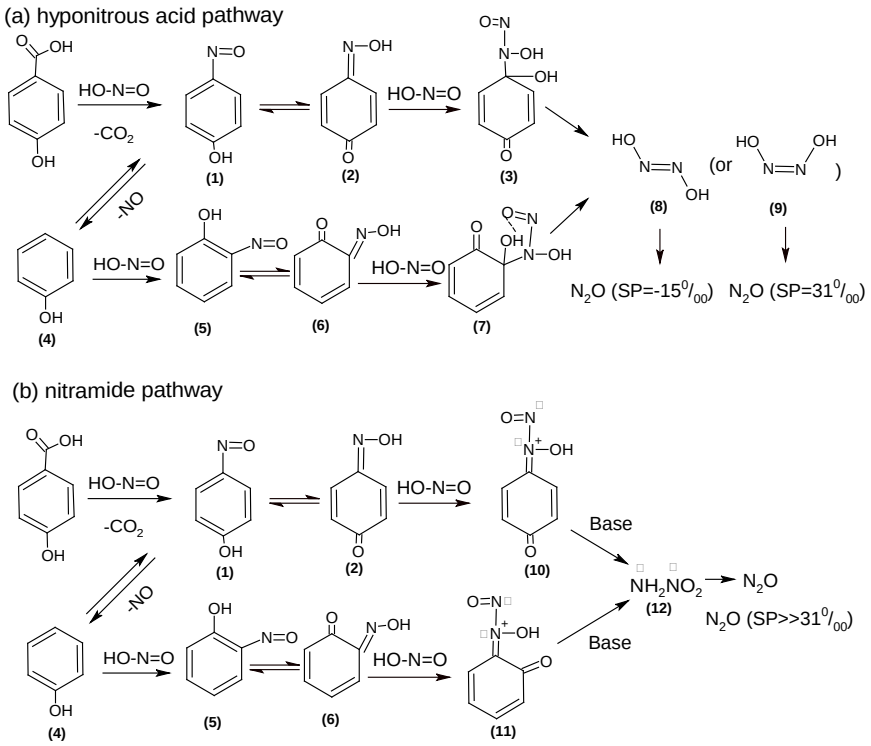

587

588 **Fig. 6**. Proposed hyponitrous acid pathway (a) and nitramide pathway (b) of N_2O formation in the
589 reactions of NO_2^- with lignin derivatives. The reaction of NO_2^- with 4-hydroxybenzoic acid is taken as
590 an example.

591

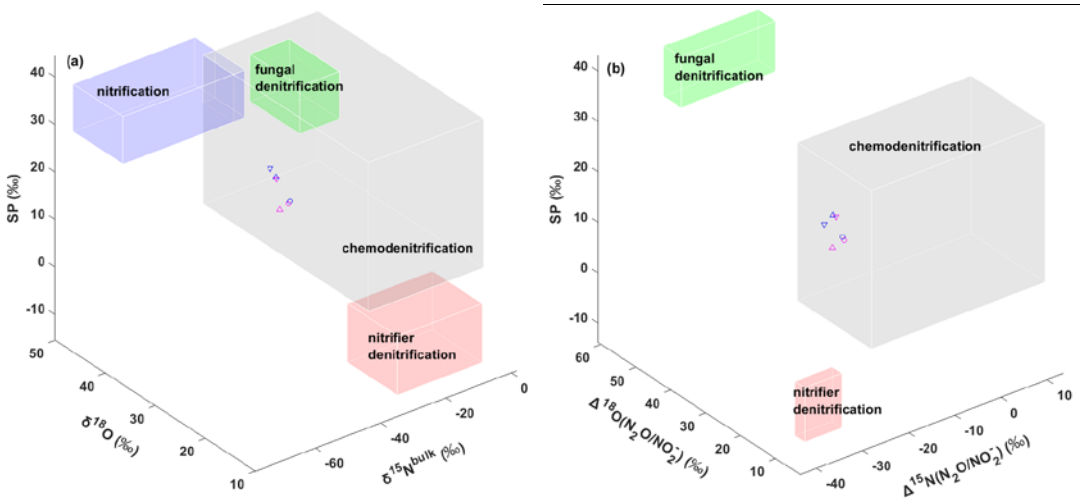

Fig. 7. Three dimensional end-member maps of N_2O isotopic signatures (a), and SP_{N2O} and net ^{15}N and ^{18}O isotopic effects (b). Pink and blue symbols represent mean values for unsterilized and sterilized soil samples, respectively. Downward triangles, agricultural soil samples; upward triangles, grassland soil samples; circles, forest soil samples.

ACKNOWLEDGEMENTS

This study was supported by the Chinese Scholarship Council (scholarship no. 201406890023), the German Federal Ministry of Education and Research (BMBF) within the frame of the INPLAMINT project (grant no. 031A561A) and the Swiss National Science Foundation (grant no. CRSII5_170876). Jing Wei was supported by the EMPAPOSTDOCS-II programme, which received funding from the European Union's Horizon 2020 research and innovation programme under the Marie Skłodowska-Curie grant agreement number 754364. The authors would like to thank Steffen Rothardt and Henning Kage at the Christian-Albrechts-Universität zu Kiel (CAU) for providing the agricultural soil, Chang Liu and Jack Hensley for helping to develop the MATLAB code for data analysis, and Kristyna Kantnerova and Patrik Zanchetta for their technical support during the experiments.

Supporting Information Available

Supporting Information. Stepwise regression of N_2O isotopocule ratios vs N_2O concentration is included.

Research Data. Wei, Jing (2019), "Data for: First real-time isotopic characterization of N2O from chemodenitrification", Mendeley Data, V1, doi: 10.17632/ntt24tgh2b.1.

REFERENCES

Austin A.T. (1961) Nitrosation in organic chemistry. *Sci. Prog.* **XLIX**, 619-640.

Berns A.E., Philipp H., Narres H.D., Burauel P., Vereecken H. and Tappe W. (2008) Effect of gamma - sterilization and autoclaving on soil organic matter structure as studied by solid state NMR, UV and fluorescence spectroscopy. *Eur. J. Soil Sci.* **59**, 540-550.

Bol R., Toyoda S., Yamulki S., Hawkins J.M.B., Cardenas L.M. and Yoshida N. (2003) Dual isotope and isotopomer ratios of N_2O emitted from a temperate grassland soil after fertiliser application. *Rapid Commun. Mass Spectrom.* **17**, 2550-2556.

Bringas M., Semelak J., Zeida A. and Estrin D.A. (2016) Theoretical investigation of the mechanism of nitroxyl decomposition in aqueous solution. *J. Inorg. Biochem.* **162**, 102-108.

Caranto J.D. and Lancaster K.M. (2017) Nitric oxide is an obligate bacterial nitrification intermediate produced by hydroxylamine oxidoreductase. *Proc. Natl. Acad. Sci. U.S.A* **114**, 8217-8222.

Chalk P.M. and Smith C.J. (1983) Chemodenitrification, in: *Gaseous loss of nitrogen from plant-soil systems* (eds. J.R. Freney, J.R. Simpson). Matinus Nijhoff, Hague.

Decock C. and Six J. (2013) How reliable is the intramolecular distribution of ^{15}N in N_2O to source partition N_2O emitted from soil? *Soil Biol. Biochem.* **65**, 114-127.

Fehling C. (2012) Mechanistic insights from the ^{15}N-site preference of nitrous oxide utilizing high resolution near-infrared cw cavity ringdown spectroscopy and density functional theory calculations. Ph. D. thesis, Kiel University.

Fehling C. and Friedrichs G. (2011) Dimerization of HNO in aqueous solution: an interplay of solvation effects, fast acid–base equilibria, and intramolecular hydrogen bonding? *J. Am. Chem. Soc.* **133**, 17912-17922.

Frame C.H. and Casciotti K.L. (2010) Biogeochemical controls and isotopic signatures of nitrous oxide production by a marine ammonia-oxidizing bacterium. *Biogeosciences* **7**, 2695-2709.

642 Grabb K.C., Buchwald C., Hansel C.M. and Wankel S.D. (2017) A dual nitrite isotopic investigation of
643 chemodenitrification by mineral-associated Fe(II) and its production of nitrous oxide. *Geochim.*
644 *Cosmochim. Acta* **196**, 388-402.
645 Gröning M. (2018) TEL Technical Note No. 01: SICalib User Manual (Stable Isotope Calibration for
646 routine δ-scale measurements) Ver 2.16j. *International Atomic Energy Agency*, Vienna, Austria.
647 Harris E., Joss A., Emmenegger L., Kipf M., Wolf B., Mohn J. and Wunderlin P. (2015) Isotopic evidence
648 for nitrous oxide production pathways in a partial nitritation-anammox reactor. Water Res. **83**,
649 258-270.
650 Heil J., Wolf B., Brüggemann N., Emmenegger L., Tuzson B., Vereecken H. and Mohn J. (2014) Site-
651 specific ^{15}N isotopic signatures of abiotically produced N_2O. *Geochim. Cosmochim. Acta* **139**,
652 72-82.
653 Heil J., Liu S., Vereecken H. and Brüggemann N. (2015) Abiotic nitrous oxide production from
654 hydroxylamine in soils and their dependence on soil properties. *Soil Biol. Biochem.* **84**, 107-115.
655 Ibraim E., Harris E., Eyer S., Tuzson B., Emmenegger L., Six J. and Mohn J. (2018) Development of a
656 field-deployable method for simultaneous, real-time measurements of the four most
657 abundant N_2O isotopocules. *Isotopes Environ. Health Stud.* **54**, 1-15.
658 IPCC (2013) Climate change 2013: The physical science basis. Contribution of working group I to the
659 fifth assessment report of the intergovernmental panel on climate change. Cambridge
660 University Press, Cambridge, United Kingdom and New York, NY, USA.
661 Jones L.C., Peters B., Pacheco J.S.L., Casciotti K.L. and Fendorf S. (2015) Stable isotopes and iron oxide
662 mineral products as markers of chemodenitrification. *Environ. Sci. Technol.* **49**, 3444-3452.
663 Jung M.Y., Well R., Min D., Giesemann A., Park S.J., Kim J.G., Kim S.J. and Rhee S.K. (2014) Isotopic
664 signatures of N_2O produced by ammonia-oxidizing archaea from soils. *ISME J.* **8**, 1115-1125.
665 Kainz G. and Huber H. (1959) Zur Kenntnis der Reaktionen, die bei der Aminostickstoffbestimmung
666 anomale Resultate verursachen. Die Anomalie der Isonitrosoverbindungen. *Microchim. Acta*
667 **47**, 337-345.

668 Kaiser K. and Benner R. (2012) Characterization of lignin by gas chromatography and mass
669 spectrometry using a simplified CuO oxidation method. *Anal. Chem.* **84**, 459-464.
670 Kool D.M., Wrage N., Oenema O., Dolfing J. and Van Groenigen J.W. (2007) Oxygen exchange between
671 (de)nitrification intermediates and H_2O and its implications for source determination of NO_3^-
672 and N_2O: a review. *Rapid Commun. Mass Spectrom.* **21**, 3569-3578.
673 Kool D.M., Wrage N., Oenema O., Harris D. and Van Groenigen J.W. (2009) The ^{18}O signature of
674 biogenic nitrous oxide is determined by O exchange with water. *Rapid Commun. Mass*
675 *Spectrom.* **23**, 104-108.
676 Kool D.M., Wrage N., Oenema O., Van Kessel C. and Van Groenigen J.W. (2011) Oxygen exchange with
677 water alters the oxygen isotopic signature of nitrate in soil ecosystems. *Soil Biol. Biochem.* **43**,
678 1180-1185.
679 Lewicka-Szczebak D., Augustin J., Giesemann A. and Well R. (2017) Quantifying N_2O reduction to N_2
680 based on N_2O isotopocules – validation with independent methods (helium incubation and ^{15}N
681 gas flux method). *Biogeosciences* **13**, 711-732.
682 Lewicka-Szczebak D., Dyckmans J., Kaiser J., Marca A., Augustin J. and Well R. (2016) Oxygen isotope
683 fractionation during N_2O production by soil denitrification. *Biogeosciences* **13**, 1129-1144.
684 Liu S., Han P., Hink L., Prosser J.I., Wagner M. and Brüggemann N. (2017) Abiotic conversion of
685 extracellular NH_2OH contributes to N_2O emission during ammonia oxidation. *Environ. Sci.*
686 *Technol.* **51**, 13122-13132.
687 Maharjan B. and Venterea R.T. (2013) Nitrite intensity explains N management effects on N_2O
688 emissions in maize. *Soil Biol. Biochem.* **66**, 229-238.
689 Mandernack K., mills, Johnson C. and Rahn T. (2009) The $\delta^{15}N$ and $\delta^{18}O$ values of N_2O produced during
690 the co-oxidation of ammonia by methanotrophic bacteria. *Chem. Geol.* **267**, 96-107.
691 Mohn J., Wolf B., Toyoda S., Lin C.T., Liang M.C., Bruggemann N., Wissel H., Steiker A.E., Dyckmans J.,
692 Szwec L., Ostrom N.E., Casciotti K.L., Forbes M., Giesemann A., Well R., Doucett R.R., Yarnes
693 C.T., Ridley A.R., Kaiser J. and Yoshida N. (2014) Interlaboratory assessment of nitrous oxide

694 isotopomer analysis by isotope ratio mass spectrometry and laser spectroscopy: current status
695 and perspectives. *Rapid Commun. Mass Spectrom.* **28**, 1995-2007.
696 Obayashi E., Takahashi S. and Shiro Y. (1998) Electronic structure of reaction intermediate of
697 cytochrome P450nor in its nitric oxide reduction. *J. Am. Chem. Soc.* **120**, 12964-12965.
698 Ostrom N.E., Gandhi H., Trubl G. and Murray A.E. (2016) Chemodenitrification in the cryoecosystem of
699 Lake Vida, Victoria Valley, Antarctica. *Geobiology* **14**, 575-587.
700 Ostrom N.E., Pitt A., Sutka R., Ostrom P.H., Grandy A.S., Huizinga K.M. and Robertson G.P. (2007)
701 Isotopologue effects during N_2O reduction in soils and in pure cultures of denitrifiers. *J.*
702 *Geophys. Res. Biogeosci.* **112**, G02005.
703 Peters B., Casciotti K.L., Samarkin V.A., Madigan M.T., Schutte C.A. and Joye S.B. (2014) Stable isotope
704 analyses of NO_2^-, NO_3^-, and N_2O in the hypersaline ponds and soils of the McMurdo Dry Valleys,
705 Antarctica. *Geochim. Cosmochim. Acta* **135**, 87-101.
706 Ravishankara A.R., Daniel J.S. and Portmann R.W. (2009) Nitrous oxide (N_2O): the dominant ozone-
707 depleting substance emitted in the 21st century. *Science* **326**, 123-125.
708 Röckmann T. and Levin I. (2005) High-precision determination of the changing isotopic composition of
709 atmospheric N_2O from 1990 to 2002. *J. Geophys. Res.* **110**, D21304.
710 Rohe L., Anderson T.H., Braker G., Flessa H., Giesemann A., Lewicka-Szczebak D., Wrage-Mönnig N. and
711 Well R. (2014) Dual isotope and isotopomer signatures of nitrous oxide from fungal
712 denitrification – a pure culture study. *Rapid Commun. Mass Spectrom.* **28**, 1893-1903.
713 Rohe L., Well R. and Lewicka-Szczebak D. (2017) Use of oxygen isotopes to differentiate between
714 nitrous oxide produced by fungi or bacteria during denitrification. *Rapid Commun. Mass*
715 *Spectrom.* **31**, 1297-1312.
716 Samarkin V.A., Madigan M.T., Bowles M.W., Casciotti K.L., Priscu J.C., McKay C.P. and Joye S.B. (2010)
717 Abiotic nitrous oxide emission from the hypersaline Don Juan Pond in Antarctica. *Nat. Geosci.*
718 **3**, 341-344.

719 Santoro A.E., Buchwald C., McIlvin M.R. and Casciotti K.L. (2011) Isotopic signature of N_2O produced
720 by marine ammonia-oxidizing archaea. Science **333**, 1282-1285.
721 Snider D.M., Schiff S.L. and Spoelstra J. (2009) $^{15}N/^{14}N$ and $^{18}O/^{16}O$ stable isotope ratios of nitrous oxide
722 produced during denitrification in temperate forest soils. Geochim. Cosmochim. Acta **73**, 877-
723 888.
724 Snider D.M., Venkiteswaran J.J., Schiff S.L. and Spoelstra J. (2015) From the ground up: Global nitrous
725 oxide sources are constrained by stable isotope values. *PLoS ONE* **10**, e0118954.
726 Stein L.Y. (2011) Surveying N_2O producing pathways in bacteria. *Methods Enzymol.* **486**, 131-152.
727 Stevenson F.J. and Swaby R.J. (1964) Nitrosation of soil organic matter: I. Nature of gases evolved
728 during nitrous acid treatment of lignins and humic substances. *Soil Sci. Soc. Am. J.* **28**, 773-778.
729 Sutka R.L., Adams G.C., Ostrom N.E. and Ostrom P.H. (2008) Isotopologue fractionation during N_2O
730 production by fungal denitrification. *Rapid Commun. Mass Spectrom.* **22**, 3989-3996.
731 Sutka R.L., Ostrom N.E., Ostrom P.H., Breznak J.A., Gandhi H., Pitt A.J. and Li F. (2006) Distinguishing
732 nitrous oxide production from nitrification and denitrification on the basis of isotopomer
733 abundances. *Appl. Environ. Microbiol.* **72**, 638-644.
734 Sutka R.L., Ostrom N.E., Ostrom P.H., Gandhi H. and Breznak J.A. (2003) Nitrogen isotopomer site
735 preference of N_2O produced by *Nitrosomonas europaea* and *Methylococcus capsulatus* Bath.
736 *Rapid Commun. Mass Spectrom.* **17**, 738-745.
737 Thevenot M., Dignac M.F. and Rumpel C. (2010) Fate of lignins in soils: A review. *Soil Biol. Biochem.* **42**,
738 1200-1211.
739 Toyoda S., Iwai H., Koba K. and Yoshida N. (2009) Isotopomeric analysis of N_2O dissolved in a river in
740 the Tokyo metropolitan area. *Rapid Commun. Mass Spectrom.* **23**, 809-821.
741 Toyoda S., Kuroki N., Yoshida N., Ishijima K., Tohjima Y. and Machida T. (2013) Decadal time series of
742 tropospheric abundance of N_2O isotopomers and isotopologues in the Northern Hemi-sphere
743 obtained by the long-term observation at Hateruma Island, Japan. *J. Geophys. Res.* **118**, 3369-
744 3381.

745 Toyoda S., Mutobe H., Yamagishi H., Yoshida N. and Tanji Y. (2005) Fractionation of N_2O isotopomers
746 during production by denitrifier. *Soil Biol. Biochem.* **37**, 1535-1545.
747 Toyoda S., Yano M., Nishimura S.-i., Akiyama H., Hayakawa A., Koba K., Sudo S., Yagi K., Makabe A.,
748 Tobari Y., Ogawa N.O., Ohkouchi N., Yamada K. and Yoshida N. (2011) Characterization and
749 production and consumption processes of N_2O emitted from temperate agricultural soils
750 determined via isotopomer ratio analysis. *Global Biogeochem. Cy.* **25**, GB2008.
751 Toyoda S. and Yoshida N. (1999) Determination of nitrogen isotopomers of nitrous oxide on a modified
752 isotope ratio mass spectrometer. *Anal. Chem.* **71**, 4711-4718.
753 Toyoda S., Yoshida N., Miwa T., Matsui Y., Yamagishi H., Tsunogai U., Nojiri Y. and Tsurushima N. (2002)
754 Production mechanism and global budget of N_2O inferred from its isotopomers in the western
755 North Pacific. *Geophys. Res. Lett.* **29**, 7-1-7-4.
756 Venterea R.T. (2007) Nitrite-driven nitrous oxide production under aerobic soil conditions: kinetics and
757 biochemical controls. *Global Change Biol.* **13**, 1798-1809.
758 Waechter H., Mohn J., Tuzson B., Emmenegger L. and Sigrist M.W. (2008) Determination of N_2O
759 isotopomers with quantum cascade laser based absorption spectroscopy. *Opt. Express* **16**,
760 9239-9244.
761 Wankel S.D., Ziebis W., Buchwald C., Charoenpong C., de Beer D., Dentinger J., Xu Z. and Zengler K.
762 (2017) Evidence for fungal and chemodenitrification based N_2O flux from nitrogen impacted
763 coastal sediments. *Nat. Commun.* **8**, 15595.
764 Watmough N.J., Field S.J., Hughes R.J. and Richardson D.J. (2009) The bacterial respiratory nitric oxide
765 reductase. *Biochem. Soc. Trans.* **37**, 392-399.
766 Wei J., Amelung W., Lehndorff E., Schloter M., Vereecken H. and Brüggemann N. (2017a) N_2O and NO_x
767 emissions by reactions of nitrite with soil organic matter of a Norway spruce forest.
768 *Biogeochemistry* **132**, 1-18.

769 Wei J., Zhou M., Vereecken H. and Brüggemann N. (2017b) Large variability of CO_2 and N_2O emissions
770 and of ^{15}N site preference of N_2O from reactions of nitrite with lignin and its derivatives at
771 different pH. *Rapid Commun. Mass Spectrom.* **31**, 1333-1343.
772 Werle P., Mucke R. and Slemr F. (1993) The limits of signal averaging in atmospheric trace-gas
773 monitoring by tunable diode-laser absorption-spectroscopy (TDLAS). *Appl. Phys. B* **57**, 131-139.
774 WMO (2016) WMO Greenhouse Gas Bulletin: The state of greenhouse gases in the atmosphere based
775 on global observations through 2015. World Meteorological Organization, Geneva.
776 Wolf B., Merbold L., Decock C., Tuzson B., Harris E., Six J., Emmenegger L. and Mohn J. (2015) First on-
777 line isotopic characterization of N_2O above intensively managed grassland. *Biogeosciences* **12**,
778 2517-2531.
779 Wunderlin P., Lehmann M.F., Siegrist H., Tuzson B., Joss A., Emmenegger L. and Mohn J. (2013) Isotope
780 signatures of N_2O in a mixed microbial population system: Constraints on N_2O producing
781 pathways in wastewater treatment. *Environ. Sci. Technol.* **47**, 1339-1348.
782 Yamazaki T., Hozuki T., Arai K., Toyoda S., Koba K., Fujiwara T. and Yoshida N. (2014) Isotopomeric
783 characterization of nitrous oxide produced by reaction of enzymes extracted from nitrifying
784 and denitrifying bacteria. *Biogeosciences* **11**, 2679-2689.
785 Yoshida N. (1988) ^{15}N-depleted N_2O as a product of nitrification. Nature **335**, 528-529.
786 Zacharias S., Bogena H., Samaniego L., Mauder M., Fuß R., Pütz T., Frenzel M., Schwank M., Baessler
787 C., Butterbach-Bahl K., Bens O., Borg E., Brauer A., Dietrich P., Hajnsek I., Helle G., Kiese R.,
788 Kunstmann H., Klotz S., Munch J.C., Papen H., Priesack E., Schmid H.P., Steinbrecher R.,
789 Rosenbaum U., Teutsch G. and Vereecken H. (2011) A Network of Terrestrial Environmental
790 Observatories in Germany. *Vadose Zone J.* **10**, 955-973.
791 Zhang W., Li Y., Xu C., Li Q. and Lin W. (2016) Isotope signatures of N_2O emitted from vegetable soil:
792 Ammonia oxidation drives N_2O production in NH_4^+-fertilized soil of North China. *Sci. Rep.* **6**,
793 29257.

794 Zhu-Barker X., Cavazos A.R., Ostrom N.E., Horwath W.R. and Glass J.B. (2015) The importance of abiotic
795 reactions for nitrous oxide production. *Biogeochemistry* **126**, 251-267.
796 Zou Y., Hirono Y., Yanai Y., Hattori S., Toyoda S. and Yoshida N. (2014) Isotopomer analysis of nitrous
797 oxide accumulated in soil cultivated with tea (*Camellia sinensis*) in Shizuoka, central Japan. *Soil*
798 *Biol. Biochem.* **77**, 276-291.